# Structure of Ternary Aluminum Metaphosphate Glasses

**ARTICLE** *in* THE JOURNAL OF PHYSICAL CHEMISTRY C · DECEMBER 2011

Impact Factor: 4.77



**4 AUTHORS**, INCLUDING:

Jefferson Esquina Tsuchida

Universidade Federal de Lavras (UFLA)

**10** PUBLICATIONS **31** CITATIONS

SEE PROFILE

Jose Fabian Schneider

University of São Paulo

**58** PUBLICATIONS **598** CITATIONS

SEE PROFILE

Hellmut Eckert

University of Münster

**536** PUBLICATIONS **9,104** CITATIONS

SEE PROFILE

THE JOURNAL OF PHYSICAL CHEMISTRY C

ARTICLE

pubs.acs.org/JPCC

# Structure of Ternary Aluminum Metaphosphate Glasses

J. Tsuchida,[†] J. Schneider,[*,†] Matthias T. Rinke,[‡] and H. Eckert[‡]

[†]Instituto de Física de São Carlos, Universidade de São Paulo, Av. Trabalhador Saocarlense 400, CEP 13566-590, São Carlos, SP, Brazil

[‡]Institut für Physikalische Chemie, Westfälische Wilhelms-Universität Münster, Corrensstrasse 30, 48149, Münster, Germany

Supporting Information

**ABSTRACT:** Ternary metaphosphate glasses in the systems $(1-x)NaPO_3 \cdot xAl(PO_3)_3$, $(1-x)KPO_3 \cdot xAl(PO_3)_3$, and $(1-x)$-$Pb(PO_3)_2 \cdot xAl(PO_3)_3$ $(0 \le x \le 1)$ were analyzed using a set of $^{31}P$, $^{27}Al$, and $^{23}Na$ high-resolution NMR and X-ray photoelectron spectroscopy techniques, to determine the phosphate speciation and the short- and medium-range order properties of the P and Al connectivity. O-1s XPS data confirm that the number of oxygen atoms linking two phosphorus remains close to 33% for all of the glasses, consistent with the exclusive presence of $Q^2$ units, in agreement with $^{31}P$ MAS NMR data. The increasing formation of Al−O−P linkages with increasing $x$ is indicated by a new O-1s peak, with binding energies near 532 eV, and systematic changes in the $^{31}P$ MAS NMR chemical shifts. The presence of $Q^2_m$ phosphate groups ($m$ being the number of P−O−Al bonds per tetrahedron, $0 \le m \le 2$) was analyzed by $^{31}P$ MAS NMR and $^{31}P\{^{27}Al\}$ REAPDOR experiments. The REDOR technique was applied to the heteronuclear spin systems $^{31}P/^{27}Al$ and $^{31}P/^{23}Na$, to analyze the local structure around these species. $^{27}Al$ MAS NMR and $^{27}Al$ triple quantum MAS were applied respectively to determine the coordination state of Al and the values of isotropic chemical shift and electric quadrupole coupling parameters of $^{27}Al$. The results points to common features in the glass structure of these ternary phosphates. The most probable environment of Al has six close P atoms, with no evidence of Al−O−Al bonds, showing that the connection between $AlO_n$ and $PO_4$ is attained through corners. There is no evidence of local segregation of cationic species in the phosphate matrix. A definite precedence in the formation of $Q^2_m$ units was found as the Al concentration is increased, consisting of the progressive conversion of $Q^2_0$ to $Q^2_1$ and then $Q^2_1$ to $Q^2_2$ units with increasing $x$. Up to intermediate values of $x$, the speciation shows an above-random trend compatible with a binary distribution $\{Q^2_0, Q^2_1\}$ for the K−Al and Pb−Al systems.

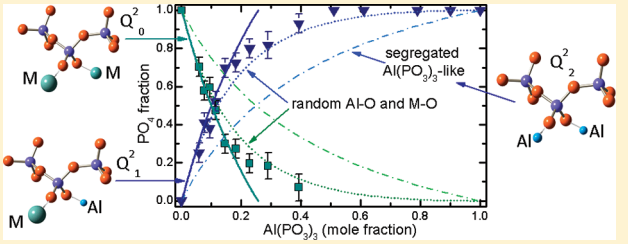


## I. INTRODUCTION

Phosphate glasses have particular properties, such as low glass transition ($T_g$) and dilatometric softening temperatures, high thermal expansion coefficients (TEC), and high UV transparency, that make them suitable for applications as low-temperature seals,[1−3] solid-state laser matrices,[4−6] confinement media for radioactive wastes,[7,8] and bioglasses.[9] The low chemical durability of phosphate glasses can be substantially improved by additional network formers and intermediate oxides, most notably aluminum.[10,11] Other species, such as alkali atoms and lead, can be incorporated in phosphate glasses at high concentrations to preserve the low-$T_g$ and high-TEC characteristics.[12]

Many properties of these materials have a direct relation with the short- and medium-range structure of the glass network. A basic structural description of phosphate glasses should specify the distribution of tetrahedral $PO_4$ species, as classified according to the number $n$ of mutual P−O−P bridges ($n$ = 0, ..., 3). These phosphate species are identified according to the notation $Q^n$. The relative abundance of $Q^n$ species in a glass can be quantified by several techniques, with high-resolution $^{31}P$ nuclear magnetic resonance (NMR) as the most conspicuous one.[13] Starting from $P_2O_5$ glass, containing only $Q^3$ groups, the addition of a modifier oxide such as $Na_2O$ creates nonbridging oxygens (NBO) that depolymerize the tetrahedral network, generating $Q^n$ groups of decreased P−O−P connectivity.[14] In the vast majority of simple phosphate glasses, the distribution of species is close to binary, i.e., at most two types of $Q^n$ units are formed at any given composition, with some effects of disproportionation depending on composition and glass processing conditions.[14,15] The evolution of the depolymerization depends on the concentration of the modifier oxide and on the valence and coordination number of the modifier species.[14,16] The mechanisms governing these structural processes and their manifestation in the evolution of glass properties have been satisfactorily explained in binary phosphate glasses.[16] The fundamental idea is that some preferential local structural arrangements around the modifier cation M determine the evolution of the medium-range structure. One key factor is the relation between the coordination number of the cation ($CN_M$) and the ratio of terminal oxygen per $PO_4$ tetrahedron, which are the O atoms interacting strongly with the modifier cation. If the concentration of terminal oxygens is sufficient to satisfy the coordination demands of the modifier cation, the preferred structural

**Received:** June 17, 2011
**Revised:** September 20, 2011
**Published:** October 03, 2011

Table 1. Analyzed Compositions for $(1-x)MPO_3 \cdot xAl(PO_3)_3$ glasses with M = Na, K in mol % and Glass Transition Temperatures in Selected K−Al Glasses[a]

| K−Al molar fraction ($x$) | $K_2O$ mol % | $Al_2O_3$ mol % | $P_2O_5$ mol % | O/P | $T_g$ (°C) | Na−Al molar fraction ($x$) | $Na_2O$ mol % | $Al_2O_3$ mol % | $P_2O_5$ mol % | O/P |
|---|---|---|---|---|---|---|---|---|---|---|
| 0 | 48 | 0 | 52 | 2.8 | 213 | 0 | 43 | 0 | 57 | 3.0 |
| 0.03 | 46 | 2 | 52 | 3.1 | | 0.06 | 45 | 3 | 52 | 3.0 |
| 0.07 | 44 | 4 | 53 | 3.0 | 233 | 0.08 | 42 | 4 | 54 | 2.9 |
| 0.09 | 42 | 4 | 54 | 2.9 | | 0.10 | 42 | 4 | 54 | 2.9 |
| 0.14 | 37 | 6 | 57 | 2.8 | | 0.12 | 39 | 5 | 56 | 3.0 |
| 0.24 | 30 | 9 | 60 | 3.0 | 406 | 0.15 | 37 | 5 | 58 | 2.9 |
| 0.31 | 27 | 12 | 62 | 3.0 | 452 | 0.18 | 35 | 8 | 57 | 2.9 |
| 0.35 | 25 | 14 | 61 | 2.7 | | 0.23 | 32 | 9 | 59 | 3.1 |
| 0.43 | 22 | 16 | 62 | 2.6 | 495 | 0.29 | 24 | 12 | 64 | 2.7 |
| 0.57 | 14 | 21 | 65 | 2.9 | 600 | 0.39 | 22 | 15 | 64 | 2.9 |
| 0.68 | 10 | 23 | 67 | 2.5 | | 0.51 | 17 | 18 | 65 | 3.0 |
| 0.78 | 7 | 27 | 66 | 3.1 | | 0.61 | 12 | 23 | 65 | 3.1 |
| 0.93 | 2 | 27 | 71 | 3.2 | | 0.79 | 5 | 33 | 62 | 2.9 |
| 1 | 0 | 28 | 72 | 2.7 | | 0.90 | 2 | 30 | 68 | 3.0 |

[a] Uncertainties in $T_g$ are ±5 °C.

arrangement in the glass involves linkages through terminal O between $PO_4$ tetrahedra and dispersed $MO_n$ groups, thus forming a corner-sharing network of coordination polyhedra. As the concentration of the oxide is increased, for compositions where the concentration of terminal oxygen atoms becomes smaller than the number required for full coordination of the modifier cation, the $MO_n$ polyhedra are forced to share corners, edges, or even faces.[16] Such a systematic description is still lacking in ternary phosphates due to the structural complexities introduced by the presence of a second chemical species. However, results obtained in Na−Al, Ca−Al, and Pb−Al metaphosphates indicate that similar principles of structural organization may be also applicable to ternary glasses.[17−19] In Al−metaphosphates (O/P = 3) it is possible to resolve different kinds of $Q^2$ phosphate species according to the number $m$ of NBO bound to Al ($m$ = 0, 1, 2), which will be identified here using the notation $Q^2_m$. These species can be partially resolved by $^{31}P$ NMR because the $^{31}P$ resonance is usually more strongly shifted by the more covalent O−Al bonds than by the weaker O−M bonds with the alkali or alkaline earth cations.[20] From the observed evolution of the populations of $Q^2_m$ species with Al in these systems, two local ordering principles were proposed for glasses up to intermediate Al concentrations:[17,19] (i) only one NBO bridge per tetrahedron is established with Al and (ii) there are no Al−O−Al bridges. Condition i, observed for glasses with low to intermediate Al content, is equivalent to the existence of a two-species distribution $\{Q^2_0, Q^2_1\}$ of aluminum−phosphate groups sharing corners. This behavior suggests the possibility that the population of $Q^2_m$ groups in phosphates may also follow a binary distribution over the entire compositional range, implying that $Q^2_0$, $Q^2_1$, and $Q^2_2$ are never simultaneously coexisting as the Al concentration is increased. In order to verify the generality of this hypothesis, the $Q^n_m$ distribution and the local/medium-range order around P and Al of many different ternary glasses should be carefully analyzed.

In this work, the ternary metaphosphate glasses $NaPO_3$−$Al(PO_3)_3$, $KPO_3$−$Al(PO_3)_3$, and $Pb(PO_3)_2$−$Al(PO_3)_3$ are analyzed using a set of $^{31}P$, $^{27}Al$, and $^{23}Na$ NMR techniques in order to determine the kind of phosphate speciation and other related structural properties of these systems. A previous NMR study on K−Al phosphates considered only the compositions $0.5K_2O \cdot xAl_2O_3 \cdot (0.5 - x)P_2O_5$ with $0.025 \leq x \leq 0.2$, starting with an O/P ratio above the metaphosphate line.[21] Previous NMR studies of the structure of Na−Al and Pb−Al metaphosphates[17,19] are extended in this work with the use of double-resonance techniques and, in the case of the Na−Al system, by analyzing samples with higher Al concentrations and using faster magic angle spinning (MAS) in $^{31}P$ and $^{27}Al$ NMR experiments. The application of special techniques to probe the heteronuclear magnetic dipolar coupling between $^{31}P/^{23}Na$ and $^{31}P/^{27}Al$ nuclear spin species, such as rotational echo double resonance (REDOR) and rotational echo adiabatic passage double resonance (REAPDOR), has been quite fruitful in the study of local and medium-range order in aluminum−phosphate glasses.[21−24] The analysis of the $^{31}P$−$^{27}Al$ coupling in the ternary glasses is a helpful tool to identify the presence of $Q^2_1$ and $Q^2_2$ units and to determine the environment of P atoms around Al, in order to probe two fundamental properties: the existence of a corner-sharing regime between Al and P polyhedra and the presence of Al−O−Al bonds. Complementary $^{27}Al$ MAS NMR and $^{27}Al$ triple quantum MAS (3Q-MAS) techniques are applied to analyze the local environments of Al, determining the average coordination number, the $^{27}Al$ isotropic chemical shift, and electric quadrupole coupling parameters. Further structural information is obtained using O-1s, Na-1s, K-2s, Al-2p, Pb-4f, and Pb-4d core electron X-ray photoelectron spectroscopy (XPS). Considering the whole set of data, three possible scenarios describing the structure of these systems as a function of the Al content can be discussed, comparing the predicted values for the populations of $Q^2_m$ units with those obtained experimentally.

## II. EXPERIMENTAL SECTION

Glasses in the systems $(1-x)NaPO_3 \cdot xAl(PO_3)_3$, $(1-x)$-$KPO_3 \cdot xAl(PO_3)_3$, and $(1-x)Pb(PO_3)_2 \cdot xAl(PO_3)_3$ were prepared by mixing the metaphosphate powders in the desired ratios. Commercial aluminum metaphosphate (Alfa Aesar 99%) and sodium trimetaphosphate $(NaPO_3)_3$ (Alfa Aesar 99%) were used as received. Potassium metaphosphate ($KPO_3$) was obtained by heating $K_2HPO_4$ powder (Alfa Aesar 99%) at 750 °C for 3 h in

porcelain crucibles. The resulting product was analyzed by X-ray diffraction, energy dispersive X-ray spectroscopy (EDX), and $^{31}$P NMR, revealing a mixture of two crystalline phases of $KPO_3$. Glasses were prepared by melting the metaphosphate powders in alumina crucibles at temperatures between 800 and 1550 °C for 20 min, the higher temperatures corresponding to higher concentrations of Al. Transparent glass pieces were obtained by pouring the melt on a heated brass block. In the case of $KPO_3$-rich glasses containing up to 0.20 mol fraction of $Al(PO_3)_3$, thin glass plates were produced by pressing the melt between two massive brass blocks to avoid crystallization. As some of the $KPO_3$ pieces showed partial crystallization, a careful separation of the optically more homogeneous glasses was done. X-ray diffraction and $^{31}$P NMR tests run on these samples consistently showed their amorphous state. The set of glass samples in the Pb−Al metaphosphate system considered here is the same as prepared for the study in ref 19. Glass compositions were analyzed for Na, K, Al, P, and O using an EDX spectrometer (LEO 440-EDX Oxford detector). Table 1 shows the analyzed compositions for the alkali−Al glasses. Compositions for Pb−Al glasses considered in this study are reported in ref 10. Values of molar fractions $x$ used throughout this paper correspond to the analyzed compositions. Glass transition temperatures ($T_g$) were measured in the K−Al series with a TA Instruments DSC-2910, running at a heating rate of 10 °C/min in Pt holders under Ar atmosphere. Glass densities at room temperature were measured by the Archimedes method using ethylene glycol as immersion liquid with an uncertainty of 0.05 g/cm$^3$.

X-ray photoelectron spectra (XPS) were measured using an Axis-Ultra spectrometer (Kratos, Manchester, UK) in ultrahigh vacuum (pressure < $10^{-7}$ Pa). All the glasses were powdered and pressed into small copper plates immediately before the measurement to get a smooth surface. This operation was done in an Ar-filled glovebox. The charge neutralizer was run with a filament current of 1.8 A, a charge balance of 2.3 V, and a filament bias of 1.0 V. Monochromatic Al K$\alpha$ radiation ($h\nu$ = 1486.6 eV) was used with a 15 kV accelerating voltage and 10 mA filament current. For narrow scans with high-energy resolution, a pass energy of 20 eV was applied. Further data analysis was done from the peak shape using the software CasaXPS Version 2.2.0 (Neal Fairley, www.casaxps.com). The omnipresent C-1s peak arising from pump oil impurities at the surface was used as an internal reference, and the binding energy of this C-1s peak was assumed to be 284.6 eV (referenced to its Fermi level). Experimentally obtained binding energies of the various peaks were corrected on the basis of the calibration factor calculated from the difference between the measured binding energy of the C-1s peak and its assumed value of 284.6 eV. The raw spectra were subsequently smoothed and fitted using mixed Gaussian/Lorentzian line shapes. In the spectra of the Na-containing glasses, the Na−Auger peak at 536 eV was removed.

$^{31}$P and $^{27}$Al MAS NMR experiments were carried out at a magnetic field strength of 9.4T in a Varian UNITY Inova spectrometer using a 4 mm probe with MAS up to 12 kHz with silicon nitride rotors. For $^{31}$P NMR, $\pi/2$ pulses of 3 $\mu$s and recycle delays up to 100s were used. For $^{27}$Al NMR, $\pi/8$ pulses of 0.5 $\mu$s and recycle delays of 1s were used. $^{27}$Al triple quantum MAS experiments (3Q-MAS) were carried out to determine the values of $^{27}$Al isotropic shift $\delta_{CS}$ and the second-order quadrupolar coupling product, $P_q = e^2qQ/(1 + \eta^2/3)^{1/2}$. Here, $eq$ and $\eta$ are respectively the principal value and the asymmetry parameter of the electric field gradient tensor (efg) at the position of the nucleus, and $eQ$ is the electric quadrupole moment of the $^{27}$Al nucleus. The 3Q-MAS experiments were carried out using a Z-filtered pulse sequence[25] using pulses at a 120 kHz nutation frequency for excitation and reconversion of three-quantum coherences, followed by a soft detection pulse (nutation frequency of 10 kHz). The recycle delay used in these experiments was 1 s. From the two-dimensional 3Q-MAS spectra, the average values of $\delta_{CS}$ and $P_q$ were calculated according to a standard procedure described in ref 26 using the values of the centers of gravity in the 3Q-MAS isotropic and in the anisotropic MAS dimensions.

$^{27}$Al{$^{31}$P}, $^{23}$Na{$^{31}$P}, and $^{31}$P{$^{23}$Na} REDOR experiments were carried out in a Bruker Avance DSX-400 spectrometer at a 9.4 T magnetic field. $^{31}$P{$^{23}$Na} REDOR experiments were run at MAS of 14 kHz with the pulse sequence discussed in ref 27, which uses a single $^{23}$Na $\pi$-pulse and a train of $^{31}$P $\pi$-pulses for reintroduction of the $^{31}$P−$^{23}$Na dipolar coupling. Typical values for $\pi$-pulse duration were 6.40 and 6.00 $\mu$s for $^{23}$Na and $^{31}$P, respectively. A recycle delay of 60s was used, in combination with a presaturation train of 12 $\pi/2$ pulses. To determine the heteronuclear second moment $M_2(^{31}\mathrm{P}\{^{23}\mathrm{Na}\})$, the data were analyzed considering the relation between the relative REDOR signal and the evolution time $\tau = NT_R$

$$\frac{\Delta S}{S_0} = \frac{1}{15\pi^2}(2 + 18f_1)(NT_R)^2 M_2(^{31}\mathrm{P}\{^{23}\mathrm{Na}\}) \quad (2)$$

where $\Delta S = S_0 - S$ is the difference between the $^{23}$Na signal intensities without ($S_0$) and with ($S$) recoupling pulses on $^{31}$P. The evolution time is a multiple $N$ of the rotor period $T_R$, and $f_1$ is an excitation factor that can be estimated from the $^{23}$Na electric quadrupole coupling constant and the pulse power.[27] Expression 2 is valid for normalized REDOR difference signals $\Delta S/S_0$ up to about 0.20. The $f_1$ factor was calculated in each experiment using the SIMPSON simulation package[28] according to the procedure described in ref 27, entering the actual experimental parameters (pulse power and MAS frequency) and the values of $^{23}$Na quadrupole coupling determined from 3Q-MAS for each analyzed glass. $^{27}$Al{$^{31}$P} and $^{23}$Na{$^{31}$P} REDOR curves were measured by the standard sequence of Gullion and Schaefer[29] using the compensation technique described in ref 30. The $M_2(^{27}\mathrm{Al}\{^{31}\mathrm{P}\})$ and $M_2(^{23}\mathrm{Na}\{^{31}\mathrm{P}\})$ values were obtained by fitting a parabola to the initial REDOR curve ($\Delta S/S_o \leq 0.2$), according to the expression[30]

$$\frac{\Delta S}{S_0} = \frac{4}{3\pi^2}(NT_R)^2 M_2(\mathrm{S}\{^{31}\mathrm{P}\}) \quad (3)$$

with $^{23}$Na or $^{27}$Al as the $S$ spin species. The experiments were run at several MAS frequencies, ranging from 12 to 15 kHz, in order to have several data points for short dephasing times. Values of $\pi$ pulses were similar to those used in $^{31}$P{$^{23}$Na} REDOR experiments, and the recycle delay for the observation of $^{27}$Al or $^{23}$Na signal was 1 s.

$^{31}$P{$^{27}$Al} REAPDOR experiments were carried out in a Bruker Avance DSX-400 spectrometer at a 9.4 T magnetic field. The pulse sequence is similar to the REDOR experiment, but uses a recoupling pulse on $^{27}$Al of duration $T_R/3$ instead of a $\pi$-pulse.[31] A typical value for $^{31}$P $\pi$-pulse duration was 5.50 $\mu$s and a spinning frequency of 14 kHz was used. A recycle delay of 60 s was applied in combination with a presaturation train of 12 $\pi/2$ pulses. The $^{31}$P{$^{27}$Al} REAPDOR dephasing curves were simulated using the SIMPSON package, using the actual experimental values of the parameters on the pulse sequence. Simulations also require values for the $^{31}$P−$^{27}$Al dipolar coupling and the $^{27}$Al quadrupolar coupling constant. The dipolar coupling was

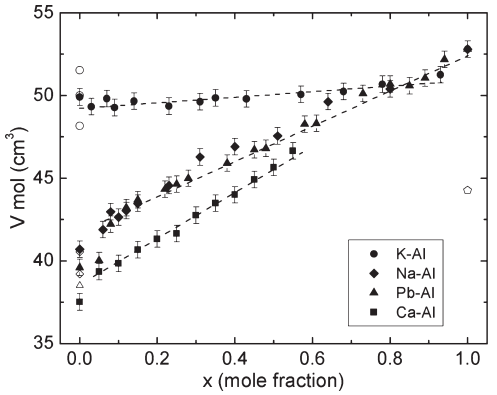


**Figure 1.** Molar volume as a function of the Al fraction in several M−Al metaphosphate glasses (M = Na, K, Ca, Pb): diamonds, Na−Al; circles, K−Al; squares, Ca−Al (data from ref 18); triangles, Pb−Al (data from ref 19); dashed lines, guides to the eye; open symbols, data for the respective crystalline Al-free metaphosphate phases; pentagon, monoclinic $Al(PO_3)_3$ crystal. Uncertainties are expressed by the bars or the size of the symbols.

estimated by assuming a P−Al distance of 3.10 Å, corresponding to the average of those observed in the monoclinic crystal form of $Al(PO_3)_3$,[32] and by considering two types of P environments separately: (i) a $^{31}P-^{27}Al$ two-spin coupling, as in $Q^2_1$ units, or (ii) a $^{31}P-^{27}Al_2$ three-spin coupling as in $Q^2_2$ units, assuming in this case an angle of 109.5° between both internuclear vectors. The relevant values for the $^{27}Al$ quadrupole coupling constant were obtained from $^{27}Al$ 3Q-MAS experiments.

Chemical shift references used in the set of NMR experiments for $^{31}P$, $^{27}Al$, and $^{23}Na$ were solutions of 85% $H_3PO_4$, 1 M $Al_2(SO_4)_3$, and 1 M NaCl, respectively.

## III. RESULTS

**Molar Volume and XPS.** The values of molar volume $V_m$ of the Na−Al and K−Al glasses were calculated using the measured mass densities. The dependence of $V_m$ with the molar fraction of $Al(PO_3)_3$ is plotted in Figure 1. Data for Pb−Al and Ca−Al metaphosphate glasses are also shown for comparison, corresponding to the sets of samples analyzed respectively in refs 18 and 19. For the Na, K, and Ca glasses, the molar volume increases linearly with the Al content, indicating that this species was uniformly incorporated into the glass network without any drastic packing rearrangement. Only for the Pb−Al system at low Al replacement ratio is there a nonlinear evolution, which seems to be associated with a structural similarity of this glass with the particularly compact structure of the $Pb(PO_3)_2$ crystal phase.[19] The small variation observed in the K−Al system is due to the similarity between the molar masses of $K_2O$ and $Al_2O_3$. Data for crystalline metaphosphates are also shown in Figure 1 (open symbols). For K and Na metaphosphates, the multiple values correspond to different crystalline phases, which are close to the $V_m$ observed in the corresponding glasses. On the other hand, the $V_m$ for the monoclinic $Al(PO_3)_3$ crystal lies well below the value for the corresponding glass, indicating substantial packing differences between both structures.

Figures 2−4 show the O-1s XP spectra for several glasses in the systems K−Al, Na−Al, and Pb−Al, respectively. The spectra were analyzed by least-squares fittings of Gaussian functions allowing the variation of all parameters. The spectra of the

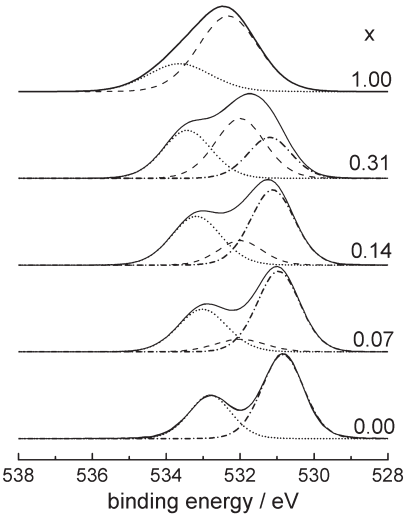


**Figure 2.** O-1s core-level photoelectron spectra of selected glass compositions in the potassium metaphosphate system. Experimental spectra are shown together with the three individual components used for fitting. Dotted curves, P−O−P species; dashed and dotted−dashed curves, nonbridging oxygen atoms linking to Al and K, respectively.

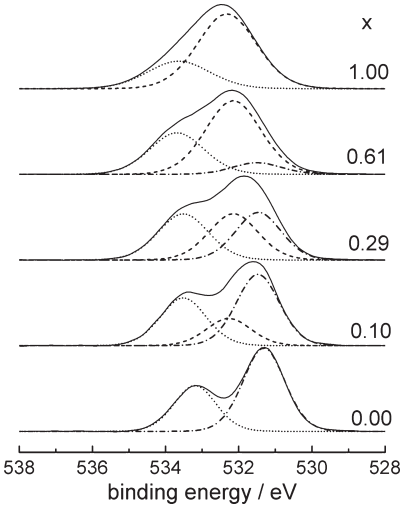


**Figure 3.** O-1s core-level photoelectron spectra of selected glass compositions in the sodium metaphosphate system. Experimental spectra are shown together with the three individual components used for fitting. Dotted curves, P−O−P species; dashed and dotted−dashed curves, nonbridging oxygen atoms linking to Al and Na, respectively.

alumina-free glasses ($x = 0$) are well-reproduced by two Gaussians, with binding energies centered near 531 and 533 eV, which can be attributed to nonbridging (P−O−M, M = K, Na, Pb) and bridging oxygen atoms (P−O−P species), respectively.[33,34] The peak area ratio is close to 2:1, as expected for glasses with metaphosphate composition. Successive (formal) substitution of the M cation by Al leads to the appearance of a new species near 532 eV, which can be attributed to nonbridging oxygen atoms forming P−O−Al instead of P−O−M linkages. Tables 2−4 list all the relevant fitting parameters for the three glass systems. The position of this peak is in good agreement with that used previously for fitting the O-1s spectra of $NaPO_3-Al_2O_3$ glasses by Brow and co-workers.[34] Its fractional area increases with


dx.doi.org/10.1021/jp205700j |J. Phys. Chem. C 2011, 115, 21927–21941

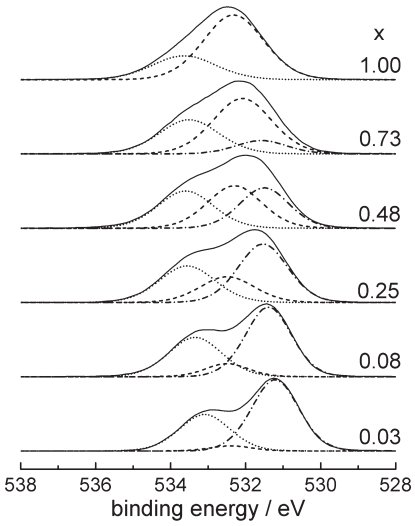


**Figure 4.** O-1s core-level photoelectron spectra of selected glass compositions in the lead metaphosphate system. Experimental spectra are shown together with the three individual components used for fitting. Dotted curves, P−O−P species; dashed and dotted−dashed curves, nonbridging oxygen atoms linking to Al and Pb, respectively.

**Table 2. Binding Energies (BE) (±0.2 eV) and Full Widths at Half-Maximum (fwhm) (±0.10 eV) for the O-1s Core-Level Photoelectrons Measured by XPS in $(1-x)KPO_3 \cdot xAl(PO_3)_3$ Glasses[a]**

| | BE (eV) | | | fwhm (eV) | | |
|---|---|---|---|---|---|---|
| $x$ | P−O−K | P−O−Al | P−O−P | P−O−K | P−O−Al | P−O−P |
| 0 | 530.8 | – | 532.8 | 1.3 | – | 1.5 |
| 0.07 | 531.0 | 532.0 | 533.0 | 1.4 | 1.6 | 1.6 |
| 0.14 | 531.1 | 532.0 | 533.2 | 1.4 | 1.4 | 1.6 |
| 0.31 | 531.2 | 532.0 | 533.4 | 1.4 | 1.6 | 1.5 |
| 1 | – | 532.3 | 533.6 | – | 1.9 | 2.0 |

| | P−O−K area (%) | | P−O−Al area (%) | | P−O−P area (%) | |
|---|---|---|---|---|---|---|
| $x$ | XPS | calcd | XPS | calcd | XPS | calcd |
| 0 | 66.0 | 66.7 | – | 0 | 34.0 | 33.3 |
| 0.07 | 56.1 | 57.6 | 10.2 | 9.1 | 33.7 | 33.3 |
| 0.14 | 48.8 | 46.0 | 15.8 | 20.6 | 35.4 | 33.3 |
| 0.31 | 25.2 | 28.4 | 41.6 | 38.3 | 32.9 | 33.3 |
| 1 | – | 0 | 72.0 | 66.7 | 28.0 | 33.3 |

[a] P−O−P = bridging oxygen between two $Q^2$ species. P−O−Al = nonbridging oxygen linking between P and Al. P−O−K = nonbridging oxygen linking between P and K.

increasing alumina content and is close to the fractional area expected if each Al present forms six Al−O−P linkages. The excellent agreement between experimental and expected area fractions is consistent with the absence of Al−O−Al linkages, at least as far as the six-coordinated aluminum species are concerned. It is further noteworthy to point out that the fractional peak area attributed to the P−O−P species remains constant near 33.3%, consistent with the metaphosphate composition of the entire set of glasses. Thus, the presence of large amounts of $Q^1$ species can be ruled out from these data. The spectral

**Table 3. Binding Energies (BE) (±0.2 eV) and Full Widths at Half-Maximum (fwhm) (±0.10 eV) for the O-1s and Core-Level Photoelectrons Measured by XPS in $(1-x)NaPO_3 \cdot xAl(PO_3)_3$ Glasses[a]**

| | BE (eV) | | | fwhm (eV) | | |
|---|---|---|---|---|---|---|
| $x$ | P−O−Na | P−O−Al | P−O−P | P−O−Na | P−O−Al | P−O−P |
| 0 | 531.3 | – | 533.2 | 1.3 | – | 1.3 |
| 0.1 | 531.5 | 532.3 | 533.5 | 1.4 | 1.4 | 1.5 |
| 0.29 | 531.5 | 532.1 | 533.5 | 1.5 | 1.6 | 1.6 |
| 0.61 | 531.5 | 532.2 | 533.7 | 1.6 | 1.8 | 1.8 |
| 1 | – | 532.3 | 533.6 | – | 1.9 | 2.0 |

| | P−O−Na area (%) | | P−O−Al area (%) | | P−O−P area (%) | |
|---|---|---|---|---|---|---|
| $x$ | XPS | calcd | XPS | calcd | XPS | calcd |
| 0 | 64.6 | 66.7 | – | 0 | 35.4 | 33.3 |
| 0.1 | 47.4 | 50.0 | 18.8 | 16.7 | 33.8 | 33.3 |
| 0.29 | 32.1 | 30.0 | 33.6 | 36.7 | 34.3 | 33.3 |
| 0.61 | 8.4 | 11.7 | 58.3 | 55.0 | 33.4 | 33.3 |
| 1 | – | 0 | 72.0 | 66.7 | 28.0 | 33.3 |

[a] P−O−P = bridging oxygen between two $Q^2$ species. P−O−Al = nonbridging oxygen linking between P and Al. P−O−Na = nonbridging oxygen linking between P and Na.

**Table 4. Binding Energies (BE) (±0.2 eV) and Full Widths at Half-Maximum (fwhm) (±0.10 eV) for the O-1s and Core-Level Photoelectrons Measured by XPS in $(1-x)Pb(PO_3)_2 \cdot xAl(PO_3)_3$ Glasses[a]**

| | BE (eV) | | | fwhm (eV) | | |
|---|---|---|---|---|---|---|
| $x$ | P−O−Pb | P−O−Al | P−O−P | P−O−Pb | P−O−Al | P−O−P |
| 0.03 | 531.2 | 532.4 | 533.1 | 1.5 | 1.3 | 1.6 |
| 0.08 | 531.4 | 532.5 | 533.3 | 1.4 | 1.3 | 1.7 |
| 0.25 | 531.5 | 532.5 | 533.6 | 1.6 | 1.7 | 1.7 |
| 0.48 | 531.5 | 532.3 | 533.6 | 1.5 | 1.7 | 1.7 |
| 0.73 | 531.6 | 532.1 | 533.5 | 1.6 | 1.8 | 1.9 |
| 1 | – | 532.3 | 533.6 | – | 1.9 | 2.0 |

| | P−O−Pb area (%) | | P−O−Al area (%) | | P−O−P area (%) | |
|---|---|---|---|---|---|---|
| $x$ | XPS | calcd | XPS | calcd | XPS | calcd |
| 0.03 | 62.1 | 63.7 | 3.9 | 3.0 | 34.0 | 33.3 |
| 0.08 | 54.8 | 59.0 | 9.5 | 7.7 | 35.7 | 33.3 |
| 0.25 | 45.8 | 44.4 | 22.1 | 22.2 | 32.1 | 33.3 |
| 0.48 | 31.3 | 28.0 | 36.3 | 38.7 | 32.4 | 33.3 |
| 0.73 | 11.4 | 13.2 | 54.6 | 53.5 | 34.0 | 33.3 |
| 1 | – | 0 | 72.0 | 66.7 | 28.0 | 33.3 |

[a] P−O−P = bridging oxygen between two $Q^2$ species. P−O−Al = nonbridging oxygen linking between P and Al. P−O−Pb = nonbridging oxygen linking between P and Pb.

components in the glasses with higher concentration of Al tend to be appreciably broadened, due to their wider ranges of bonding environments. For these glasses, the usefulness of the


dx.doi.org/10.1021/jp205700j |J. Phys. Chem. C 2011, 115, 21927–21941

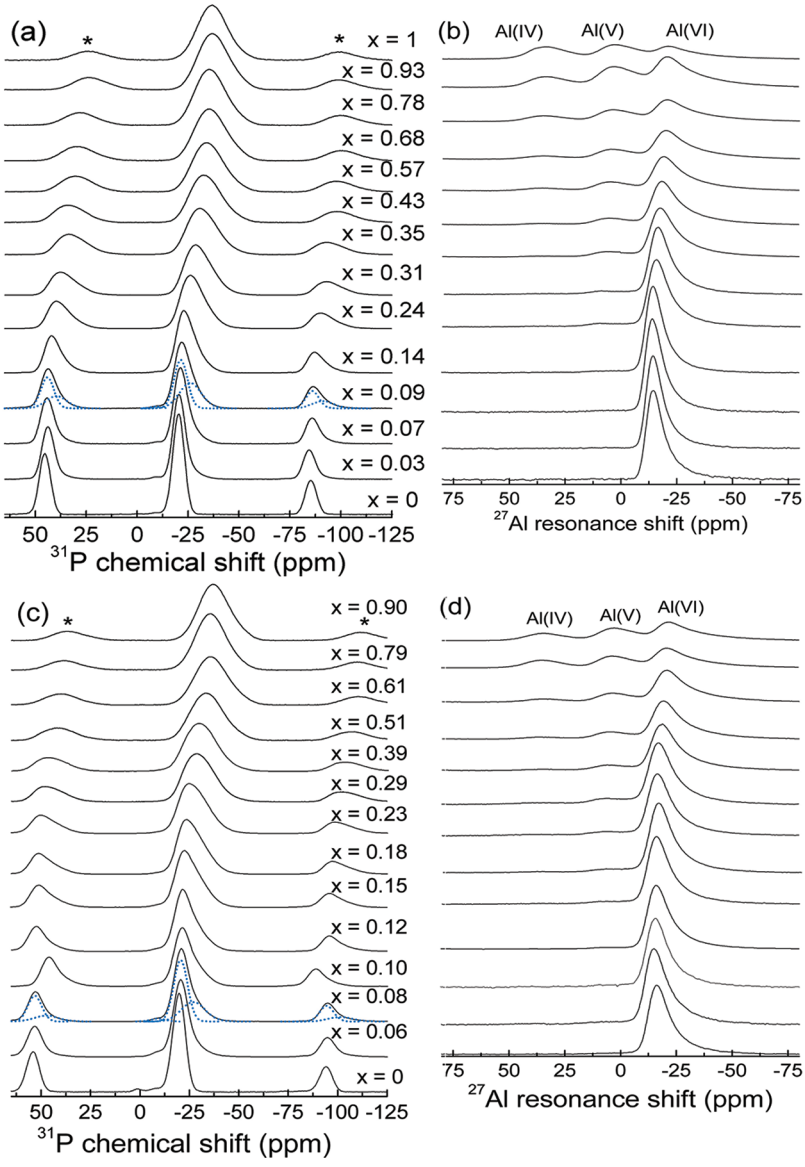


**Figure 5.** (a) $^{31}$P NMR and (b) $^{27}$Al NMR spectra in K−Al glasses. (c) $^{31}$P NMR and (d) $^{27}$Al NMR spectra in Na−Al glasses. *x*, molar fraction of $Al(PO_3)_3$; asterisks, spinning side-bands; dotted lines, examples of typical least-squares fittings of $^{31}$P NMR spectra with Gaussian functions.

calculated areas is limited, due to the more complex Al speciation revealed by $^{27}$Al NMR. The lack of enough resolution in the O-1s peak for Al−O−P precludes any detailed analysis. Figures S-1, S-2, and S-3 (Supporting Information) summarize the XP spectra for the K-2p, Na-1s, and Pb-4f and Pb-4d electrons, respectively. Tables S-4−S-6 (Supporting Information) summarize the corresponding fitting parameters as well as those of the Al-2p XPS data. For all of the elements, the binding energies determined from the spectra show a weak tendency to increase with increasing alumina content in all three systems. This trend may indicate a systematic bond strengthening for all of the phosphate bonds with increasing aluminum content. On the other hand, the possibility that this effect might be influenced by systematic variations in the degree of sample charging as a function of *x* cannot be rigorously excluded, even though all the spectra were measured under conditions of surface charge neutralization.

**NMR.** *K−Al Metaphosphate Glasses.* Figure 5a shows the $^{31}$P MAS NMR spectra obtained for this system. The observed NMR line in the $KPO_3$ glass at −20.3 ppm corresponds to $Q^2$ groups and shows a progressive shift and asymmetric broadening to lower frequencies with the increase in the Al concentration. This behavior is related to the growing number of P−O−Al bonds, creating $Q^2_1$ and $Q^2_2$ units contributing to the low-frequency side of the spectra.[20] The broadening of the lines does not allow a specific attribution of this shoulder to either $Q^2_1$ or $Q^2_2$ units. Figure 6 shows the evolution of the average $^{31}$P MAS isotropic chemical shift with composition (values in Table 5), revealing two regions with linear behavior, with an apparent break at $x \sim 0.40$ for alkali-Al glasses and $x \sim 0.48$ for Pb−Al. In each region, the linear evolution of the average shift suggests a random mixture of a certain set of phosphate species $Q^2_m$, with population fractions varying uniformly as a function of *x*. The break in the slope indicates a change of regime in the distribution of the species contributing to the average, as for example the appearance of a new species with different characteristic chemical shift. As will be discussed in section IV, this phenomenon may be


dx.doi.org/10.1021/jp205700j |*J. Phys. Chem. C* 2011, 115, 21927–21941

related to the appearance of $Q^2_2$ species above a certain critical concentration.

For glasses with low to medium Al concentration, it was possible to estimate the population fraction of $Q^2_0$ and $Q^2_m$ (with $m = 1, 2$) from the $^{31}$P spectra, fitting Gaussian functions to the central line and to the MAS sidebands at $\pm\nu_R$ and $\pm 2\nu_R$. Contributions from the $\pm 3\nu_R$ sidebands were always less than 0.5% and for this reason were disregarded. The resulting populations are shown in Table 5 and plotted in Figure 7a. These data will be analyzed in the Discussion section also considering the results for Na−Al and Pb−Al metaphosphates.

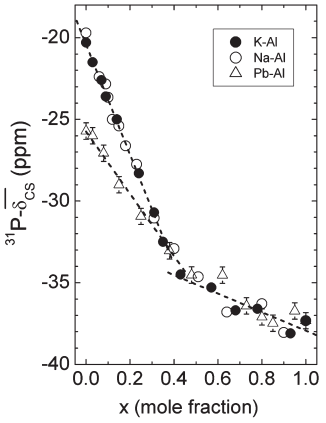


**Figure 6.** Average value for the isotropic $^{31}$P chemical shift in K−Al (filled circles), Na−Al (open circles), and Pb−Al (open triangles) metaphosphate glasses. Straight lines are guides to the eye. Uncertainties are of the size of symbols or the error bars.

Figure 5b shows the $^{27}$Al MAS NMR spectra obtained for this set of glasses, showing Al with coordination numbers 4, 5, and 6. The average coordination number CN was calculated from the areas of these resonances, giving the result shown in Figure 8. As the Al concentration increases, the CN decreases from 6 to 5 across the entire compositional range. These values will be considered in the analysis of $Q^2_m$ populations carried out in section VI. Further analysis of the Al sites was done using two-dimensional $^{27}$Al 3Q-MAS experiments to determine the isotropic chemical shift $\delta_{CS}$ and the quadrupole coupling product $P_q$. The obtained values are shown in Table 5. Figure 9 shows the variation with composition of these parameters for the Al(VI) site, which is the most abundant Al species in all the glass systems studied in this work. The linear evolution of $\delta_{CS}$ suggests uniform mixing of Al with the second cation in the phosphate matrix, rather than segregation in Al-rich domains. The increase in the $^{27}$Al magnetic shielding with the increase in the Al concentration is consistent with results obtained in other aluminophosphate glasses[35] and indicates a general behavior that will be discussed in section IV. The average quadrupolar coupling product $P_q$ (Figure 9b) increases with the concentration of Al, indicating a progressive symmetry-reducing distortion in the local geometry of the $AlO_6$ polyhedron.

Figure 10 shows some representative $^{27}$Al{$^{31}$P} REDOR curves obtained for selected compositions of the analyzed glass

**Table 5. MAS-NMR Parameters for K−Al Metaphosphate Glasses**[a]

| K−Al molar fraction ($x$) | $^{31}$P $\delta_{CG}$ (ppm) | $Q^2_0$ | $Q^2_m$ | $^{27}$Al $\delta_{iso}$ (ppm) | $^{27}$Al $P_q$ (MHz) |
|---|---|---|---|---|---|
| 0 | −20.3 ± 0.2 | 1 | 0 | | |
| 0.03 | −21.5 ± 0.2 | 0.81 ± 0.05 | 0.19 ± 0.05 | VI, −11.7 ± 0.3 | 2.4 ± 0.2 |
| 0.07 | −22.6 ± 0.2 | 0.70 ± 0.05 | 0.31 ± 0.05 | VI, −12.4 ± 0.3 | 2.0 ± 0.2 |
| 0.09 | −23.6 ± 0.2 | 0.57 ± 0.05 | 0.43 ± 0.05 | VI, −12.0 ± 0.3 | 2.3 ± 0.2 |
| 0.14 | −25.0 ± 0.2 | 0.50 ± 0.05 | 0.51 ± 0.05 | VI, −12.9 ± 0.3 | 1.9 ± 0.2 |
| 0.24 | −28.3 ± 0.2 | 0.11 ± 0.05 | 0.89 ± 0.05 | VI, −13.3 ± 0.3 | 2.7 ± 0.2 |
| 0.31 | −30.7 ± 0.2 | 0.08 ± 0.05 | 0.92 ± 0.05 | VI, −13.9 ± 0.3 | 2.7 ± 0.2 |
| 0.35 | −32.5 ± 0.2 | 0 | 1 | VI, −14.9 ± 0.3 | 3.3 ± 0.2 |
| | | | | V, 13.0 ± 0.5 | 3.1 ± 0.5 |
| 0.43 | −34.5 ± 0.2 | 0 | 1 | VI, −15.8 ± 0.3 | 3.3 ± 0.2 |
| | | | | V, 12.9 ± 0.3 | 3.0 ± 0.5 |
| 0.57 | −35.3 ± 0.2 | 0 | 1 | VI, −16.7 ± 0.3 | 3.7 ± 0.2 |
| | | | | V, 12.6 ± 0.3 | 2.9 ± 0.4 |
| 0.68 | −36.7 ± 0.2 | 0 | 1 | VI, −16.9 ± 0.3 | 3.7 ± 0.2 |
| | | | | V, 12.2 ± 0.3 | 3.2 ± 0.2 |
| | | | | IV, 44.0 ± 0.5 | 3.6 ± 0.5 |
| 0.78 | −36.6 ± 0.2 | 0 | 1 | VI, −18.7 ± 0.3 | 3.7 ± 0.2 |
| | | | | V, 11.2 ± 0.3 | 3.1 ± 0.3 |
| | | | | IV, 43.1 ± 0.5 | 3.4 ± 0.5 |
| 0.93 | −38.1 ± 0.2 | 0 | 1 | VI, −18.9 ± 0.3 | 4.1 ± 0.2 |
| | | | | V, 10.8 ± 0.5 | 3.4 ± 0.3 |
| | | | | IV, 42.1 ± 0.5 | 3.7 ± 0.3 |
| 1 | −37.3 ± 0.3 | 0 | 1 | VI, −18.9 ± 0.5 | 3.9 ± 0.2 |
| | | | | V, 9.6 ± 0.5 | 3.4 ± 0.3 |
| | | | | IV, 40.2 ± 0.5 | 3.2 ± 0.3 |

[a] $\delta_{CG}$: center of gravity of the $^{31}$P MAS-NMR line. $Q^2_0$ and $Q^2_m$: fractional populations of phosphate species determined from the $^{31}$P MAS-NMR spectra. $^{27}$Al $\delta_{iso}$ and $P_q$: isotropic chemical shift and second-order quadrupolar coupling product, respectively, determined from $^{27}$Al 3Q-MAS experiments for each kind of observed Al site (coordination VI, V, or IV).


dx.doi.org/10.1021/jp205700j |J. Phys. Chem. C 2011, 115, 21927–21941

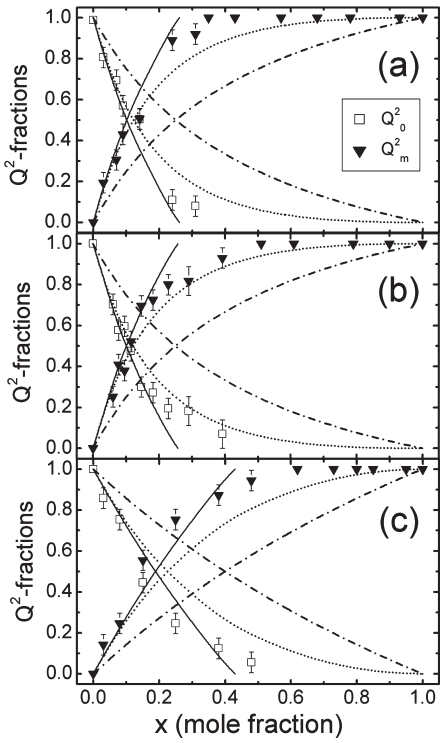


**Figure 7.** Fraction of phosphate species determined from $^{31}$P NMR and calculated according to three structural models for metaphosphate glasses: (a) K−Al, (b) Na−Al, and (c) Pb−Al (data from ref 19). Squares, $Q^2_0$ from NMR; triangles, $Q^2_m$ ($m$ = 1, 2) from NMR; full lines, calculation of $Q^2_0$ and $Q^2_1$ for a binary distribution; dotted lines, calculation of $Q^2_0$ and $Q^2_m$ for a random binomial distribution; dashed−dotted lines, calculation of $Q^2_0$ and $Q^2_2$ for a segregated distribution.

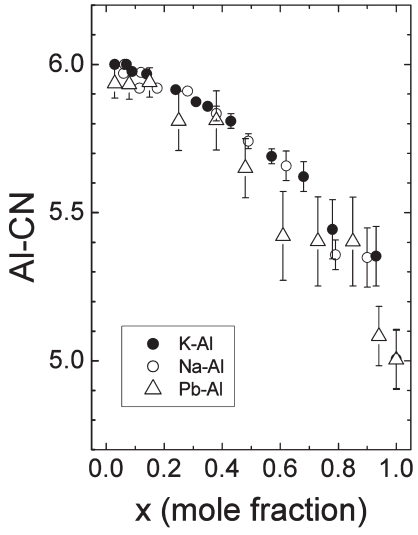


**Figure 8.** Average coordination number for Al in M−Al metaphosphate glasses obtained from $^{27}$Al NMR line intensities with M = K (filled circles), M = Na (open circles), and Pb−Al (open triangles). Data for Pb−Al metaphosphate glasses are the same as in ref 19.

systems. The curve in Figure 10a corresponds to one of the analyzed samples in the K−Al system ($x$ = 0.31). The parabolic analysis according to expression 3 yielded the $M_2(^{27}\text{Al}\{^{31}\text{P}\})$

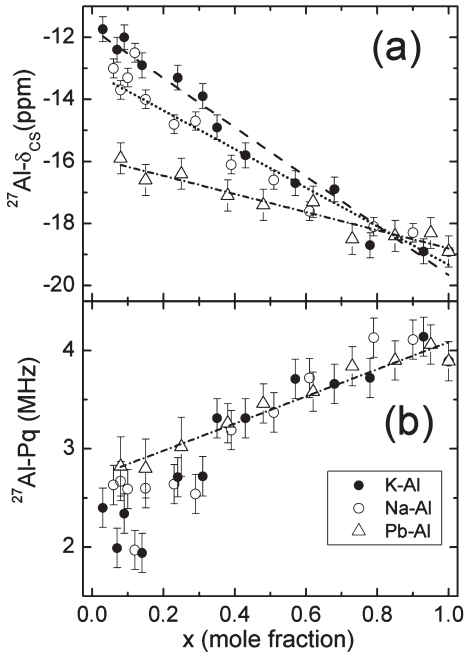


**Figure 9.** (a) $^{27}$Al Isotropic chemical shift $\delta_{CS}$ and (b) $^{27}$Al electric quadrupole coupling product $P_q$ for Al(VI) in M−Al metaphosphate glasses (M = Na, K, Pb) obtained from $^{27}$Al 3Q-MAS experiments: filled circles, K−Al; open circles, Na−Al; triangles, Pb−Al; straight lines are linear least-squares fittings for K−Al (dashed line), Na−Al (dotted line), and Pb−Al (dashed−dotted lines).

values shown in Table 6. $^{27}$Al{$^{31}$P} REDOR measurements for the $Al(PO_3)_3$ glass were carried out, as shown in Figure 10d,e,f for the three $^{27}$Al species observed, with coordination numbers VI, V, and IV, respectively. The corresponding $M_2(^{27}\text{Al}\{^{31}\text{P}\})$ values for these sites, shown in Table 6, are comparable with that obtained for Al(VI) in a sample of crystalline $Al(PO_3)_3$ in monoclinic form ($5.4 \pm 0.2 \times 10^6$ rad$^2$ s$^{-2}$). According to the set of data in Table 6, the $M_2(^{27}\text{Al}\{^{31}\text{P}\})$ values are quite similar in all the systems and no trend can be identified as a function of the composition. The lack of differences in $^{27}$Al{$^{31}$P} dipolar coupling for Al in its different coordination states may arise from two reasons: first of all, the lower number of P neighbors close to four-coordinated Al may be compensated by Al···P distances that are somewhat shorter compared to those observed for Al species in higher coordination states. This effect has been previously observed for other aluminophosphate glass systems.[23] Second, in these P-rich glasses additional contributions to $M_2$ are expected from coupling of the central $^{27}$Al with next-nearest $^{31}$P neighbors. Both of these effects probably smear out the expected dependence of $M_2$ on the number of nearest $^{31}$P neighbors to Al(IV), Al(V), and Al(VI). Therefore, it can be concluded that there is a qualitative similarity of the local order in the glasses and crystalline $Al(PO_3)_3$, which excludes the possibility of extensive Al−O−Al bonding in these systems.

Figure 11 shows $^{31}$P{$^{27}$Al} REAPDOR results obtained in $Al(PO_3)_3$ glass, applying the rf pulses on the $^{27}$Al channel on-resonance with the Al(VI) line. The data points represent the ratio $\Delta S/S_0$ obtained from the integration of the center band of the $^{31}$P spectra. Two other sets of experiments were carried out with the Al(V) and Al(IV) NMR lines irradiated on-resonance, yielding identical results. The full line in Figure 11 corresponds to the SIMPSON simulation for a three-spin system involving one

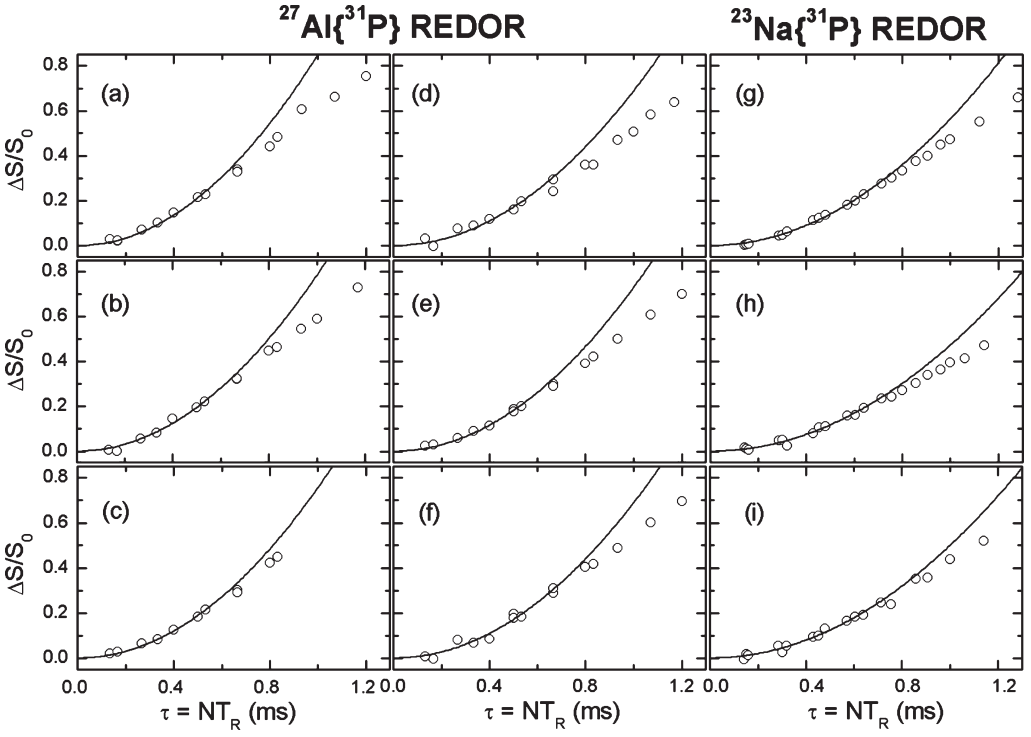


**Figure 10.** Typical $^{27}$Al{$^{31}$P} and $^{23}$Na{$^{31}$P} REDOR results in some metaphosphate glasses: (a) K−Al $x$ = 0.31, (b) Na−Al $x$ = 0.29, (c) Pb−Al $x$ = 0.48, (d) Al(VI) in Al$(PO_3)_3$, (e) Al(V) in Al$(PO_3)_3$, (f) Al(IV) in Al$(PO_3)_3$, (g) Na−Al $x$ = 0.08, (h) Na−Al $x$ = 0.29, (i) Na−Al $x$ = 0.61. Full lines: parabolic least-squares fittings considering REDOR difference signals up to 0.20.

$^{31}$P and two neighboring $^{27}$Al nuclei, assuming the P−Al distance observed in the crystalline phase. The value of $P_Q$ used in the calculation was the one measured with $^{27}$Al 3Q-MAS. The excellent agreement with the experimental data indicates that phosphate groups establish P−O−Al bonds with two different Al atoms. This situation corresponds to a connectivity regime where phosphate tetrahedra and Al polyhedra share corners, instead of edges, in full agreement with the model proposed by Hoppe.[16]

Figure 12a,b,c shows $^{31}$P{$^{27}$Al} REAPDOR results in the K−Al system for $x$ = 0.09, 0.31, and 0.68, respectively. These plots show the total difference signal $\Delta S/S_0$ (filled circles), integrated from the central band in each spectrum of the pair of REAPDOR experiments. In glasses with low concentration of Al, the amount of dephasing $\Delta S$ is most intense at the low-frequency side of the $^{31}$P spectrum. This can be seen in Figure 13a,b, which shows some of the $^{31}$P{$^{27}$Al} REAPDOR difference spectra $\Delta S$ as a function of the evolution time $\tau$. This behavior is consistent with the fact that that region of the spectrum corresponds to $Q^2_1$ or $Q^2_2$ groups, with stronger $^{31}$P−$^{27}$Al dipolar coupling than present in $Q^2_0$. However, the coupling of the latter units may not be completely negligible, because for longer times $\tau$ there is a noticeable shift of the peaks of REAPDOR difference spectra to lower frequencies (Figure 13a). For glasses with higher Al content, the shapes of the REAPDOR difference spectra are comparable with the $^{31}$P MAS spectrum for all $\tau$ (Figure 13b), without any noticeable change in the central position.

Figure 12a−c also shows the calculated $^{31}$P{$^{27}$Al} REAPDOR curves for dipolar coupling between two spins ($^{31}$P−$^{27}$Al) and three spins ($^{31}$P−$^{27}$Al$_2$). These simulations may be a good approximation for those glasses with a significant fraction of $Q^2_1$ or $Q^2_2$ units, where the eventual contribution of the more difficult to simulate $^{31}$P−$^{27}$Al coupling of $Q^2_0$ phosphorus species is minimized. Figure 12b shows the results of both simulations for the glass with $x$ = 0.31. The three-spin simulation for this experiment (dotted line) lies well above the experimental data. The two-spin simulation (dashed−dotted line) reproduces quite well the observed experimental REAPDOR data. As in this glass, the fraction of $Q^2_m$ was estimated as 0.92; the agreement of the REAPDOR evolution with the simulation without any scaling by the population factor indicates that most of the $Q^2_m$ species may be attributed to $Q^2_1$. For the $x$ = 0.68 glass (Figure 12c) the REAPDOR data lies well above the two-spin simulation and closer to the three-spin simulation, indicating that the observed response is a mixture resulting from contributions of $Q^2_1$ and $Q^2_2$ environments. The full-line curve shown in this plot is the closest approximation to the experimental data obtained as a weighed sum of both simulations, with populations of 0.25 for $Q^2_1$ and 0.75 for $Q^2_2$. For the glass with $x$ = 0.09 (Figure 12a), the experimental REAPDOR data lies below the two-spin simulation due to the presence of a significant fraction of $Q^2_0$. These latter groups have non-negligible dipolar coupling with $^{27}$Al at longer distances, which cannot be simulated in a straightforward manner.

*Na−Al Metaphosphate.* Figure 5c shows the $^{31}$P MAS NMR spectra obtained for this system. The resonance from $Q^2$ groups shows a progressive shift and a broadening with the concentration of Al, similar to that observed in the K−Al system, due to the increasing formation of P−O−Al bonds with increasing $x$. The plot of the average $^{31}$P isotropic chemical shift (Figure 6, data in Table 7), shows the same behavior as in K−Al glasses, indicating a similar change of regime in the association of P and Al at concentrations close to $x$ = 0.40. The fractions of $Q^2_0$ and $Q^2_m$ ($m$ = 1, 2) determined from Gaussian least-squares fittings to the $^{31}$P spectra are shown in Figure 7b and Table 7 and will be further


dx.doi.org/10.1021/jp205700j |*J. Phys. Chem. C* 2011, 115, 21927–21941

Table 6. Values of Second Moments $M_2(^{27}Al\{^{31}P\})$, $M_2(^{23}Na\{^{31}P\})$, $M_2(^{31}P\{^{23}Na\})$ Obtained Respectively Through $^{27}Al\{^{31}P\}$ REDOR and $^{23}Na\{^{31}P\}$ REDOR Experiments for Selected Glass Compositions in the K−Al, Na−Al, and Pb−Al Metaphosphates and a Crystalline Sample of $Al(PO_3)_3$ in Its Monoclinic Form[a]

| $x$ | $M_2(^{27}Al\{^{31}P\})$ ($10^6$ rad$^2$ s$^{-2}$) | $M_2(^{23}Na\{^{31}P\})$ ($10^6$ rad$^2$ s$^{-2}$) | $M_2(^{31}P\{^{23}Na\})$ ($10^6$ rad$^2$ s$^{-2}$) | $f_1$ |
|---|---|---|---|---|
| | | K−Al | | |
| 0.09 | VI, 5.4 ± 0.2 | | | |
| 0.31 | VI, 6.3 ± 0.2 | | | |
| | | Na−Al | | |
| 0 | | 3.3 ± 0.3 | 17 ± 1 | 0.0280 |
| 0.08 | VI, 5.5 ± 0.2 | 4.2 ± 0.3 | 16.6 ± 0.8 | 0.0579 |
| 0.29 | VI, 5.8 ± 0.2 | 3.5 ± 0.3 | 8.6 ± 0.8 | 0.0515 |
| 0.61 | VI, 5.5 ± 0.2 | 3.9 ± 0.3 | 4.2 ± 1.5 | 0.0423 |
| | | Pb−Al | | |
| 0.08 | VI, 5.5 ± 0.2 | | | |
| | VI, 5.6 ± 0.2 | | | |
| | VI, 5.0 ± 0.2 | | | |
| | V, 5.1 ± 0.2 | | | |
| | | $Al(PO_3)_3$ | | |
| | VI, 5.1 ± 0.3 | | | |
| | V, 5.4 ± 0.3 | | | |
| | IV, 5.1 ± 0.3 | | | |
| | | $Al(PO_3)_3$ crystal | | |
| | VI, 5.4 ± 0.2 | | | |

[a] Coordination of the observed Al site is indicated (VI, V, IV).

analyzed in the Discussion section. These values are compatible with those presented in ref 17.

Figure 5d shows the $^{27}Al$ MAS spectra for this series of glasses, showing lines corresponding to Al in coordination VI, V, and IV. From the line intensities, the average coordination numbers were calculated, resulting in values comparable to those measured in the K−Al system (Figure 8). The values of $^{27}Al$ $\delta_{CS}$ and $P_q$ obtained from $^{27}Al$ 3Q-MAS experiments are shown in Table 7. Figure 9 shows the evolution of these parameters for the Al(VI) sites. The linear variation of the isotropic chemical shift with the Al content, as in the case of K−Al glasses, indicates mixing of Na and Al at the atomic scale. $P_q$ increases with increasing concentration of Al, indicating a progressive distortion in the average local symmetry of the Al(VI) sites as observed in the K−Al system.

Figure 10g,h,i shows the results of $^{23}Na\{^{31}P\}$ REDOR experiments carried out in three representative glasses, with $x$ = 0.08, 0.29, and 0.61. Values of $M_2(^{23}Na\{^{31}P\})$, shown in Table 6, were obtained from parabolic least-squares fittings of expression 3 to the observed REDOR signals for short evolution times. There is no significant variation in these $M_2(^{23}Na\{^{31}P\})$ values, indicating that the local average environment of P atoms around Na is similar irrespective of the Al content in the glass.

Figure 10b shows a typical result of the $^{27}Al\{^{31}P\}$ REDOR experiments carried out in the Na−Al system, for the glass with $x$ = 0.29. Table 6 shows the $M_2(^{27}Al\{^{31}P\})$ values obtained from these experiments. As observed in the K−Al system, there is no definite trend of this parameter with composition that may

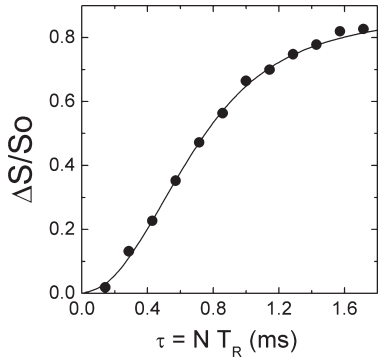


**Figure 11.** $^{31}P\{^{27}Al\}$ REAPDOR in $Al(PO_3)_3$ glass carried out irradiating with the Al(VI) NMR line on-resonance. Full line: SIMPSON simulation assuming a three-spin interaction $^{31}P-^{27}Al_2$.

indicate any drastic variation in the local environment of P atoms around Al.

Figure 12d,e,f shows the evolution of $^{31}P\{^{27}Al\}$ REAPDOR signals in three Na−Al metaphosphate glasses with compositions $x$ = 0.08, 0.29, and 0.61, respectively. All the plots show the integrated REAPDOR difference $\Delta S/S_0$ (filled circles). In general, these $^{31}P\{^{27}Al\}$ REAPDOR results are similar to the findings in the K−Al system. According to the REAPDOR difference spectra plotted in Figure 13c, the glass with $x$ = 0.08 has a spectral region with stronger $^{31}P-^{27}Al$ dipolar coupling, which corresponds to the lower frequency end of the $^{31}P$ spectrum where $Q^2_1$ and $Q^2_2$ resonances are expected. The maximum of the REAPDOR difference spectrum of this glass shifts to higher frequency for long $\tau$ values, indicating that $^{31}P$ in $Q^2_0$ groups may have a weak dipolar coupling with $^{27}Al$.

In the glass with $x$ = 0.29, a uniform response of the REDOR difference line shape with $\tau$ can be observed (figure 13d). In this case, the measured REAPDOR intensity lies below the two-spin simulation (dashed−dotted line in Figure 12e). The experimental data may be accurately reproduced by scaling the two-spin curve with a factor 0.84 (full line in Figure 12e), which agrees quite well with the $Q^2_m$ fraction of 0.82 estimated from MAS. Therefore, it can be concluded that the observed REAPDOR signal may be attributed to $Q^2_1$ groups.

For the glass with $x$ = 0.61 (Figure 12f) the experimental data lie in between the two-spin and three-spin simulations, revealing the presence of $Q^2_2$ units in the structure of this glass. A weighted combination of the three- and two-spin simulated curves reproduces the experimental evolution of the full REAPDOR signal, considering a fraction of 0.30 for $Q^2_2$.

For the glass with $x$ = 0.08, the full REAPDOR signal plotted in Figure 12d may have some non-negligible contribution from $Q^2_0$, in addition to the more strongly coupled but less abundant $Q^2_m$ units. The dashed−dotted line represents the two-spin simulation. The scaling of this curve to obtain the best approximation to the experimental data was achieved with a population factor of 0.38 (full line in Figure 12d), which is not far from the value of 0.42 estimated for the $Q^2_m$ population from $^{31}P$ MAS. Therefore, this result supports the identification of most of the Al-connected $Q^2_m$ units as units having $m$ = 1.

Figure 14 shows the $^{31}P\{^{23}Na\}$ REDOR curves obtained for the glasses with $x$ = 0.08, 0.29, and 0.61. Table 6 shows the values for $M_2(^{31}P\{^{23}Na\})$, obtained using the procedure described in section II (eq 2). The decrease of these values indicates the progressive depletion of Na neighbors around P, as the

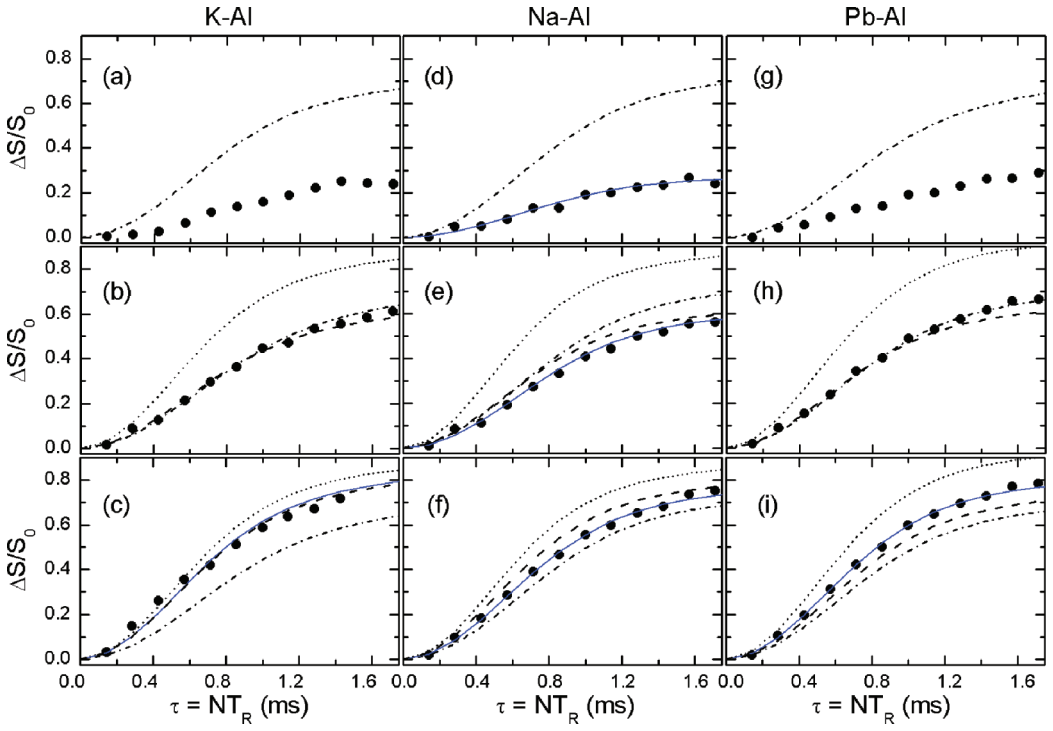


**Figure 12.** $^{31}P\{^{27}Al\}$ REAPDOR results in metaphosphate glasses. K−Al: (a) $x = 0.09$, (b) $x = 0.31$, (c) $x = 0.68$. Na−Al: (d) $x = 0.08$, (e) $x = 0.29$, (f) $x = 0.61$. Pb−Al: (g) $x = 0.08$, (h) $x = 0.48$, (i) $x = 0.80$. Filled circles, experimental REAPDOR signal; dashed−dotted lines, SIMPSON simulations for two-spin dipolar coupling ($^{31}P-^{27}Al$); dotted lines, SIMPSON simulations for three-spin dipolar coupling ($^{31}P-^{27}Al_2$); full lines, linear combination of the simulated curves weighed with population factors to fit experimental data (see text for each case); dashed lines linear combination of two- and three-spin simulations weighted with the $Q^2_1$ and $Q^2_2$ populations from the random model.

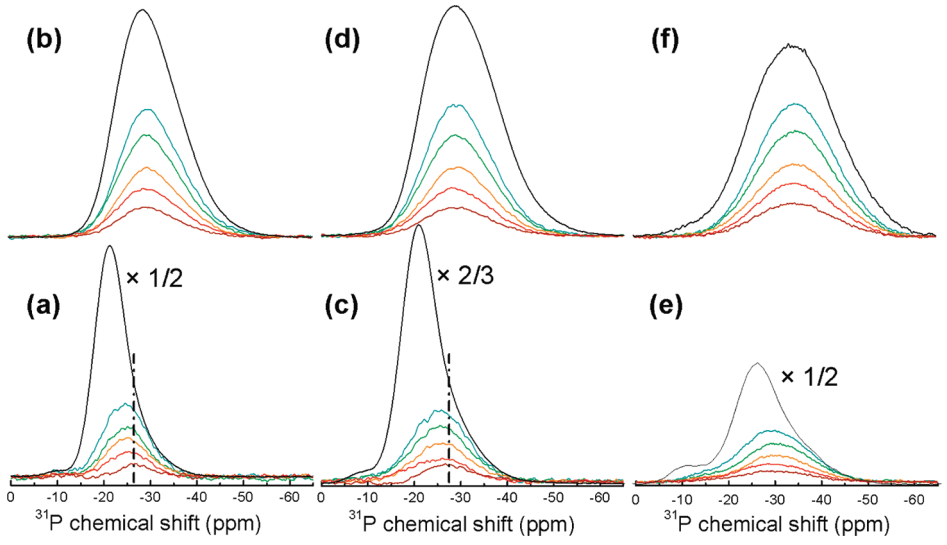


**Figure 13.** Typical $^{31}P\{^{27}Al\}$ REAPDOR difference spectra in some glasses. K−Al: (a) $x = 0.09$, (b) $x = 0.31$. Na−Al: (c) $x = 0.08$, (d) 0.29. Pb−Al: (e) $x = 0.08$ (f) $x = 0.48$. Upper trace in each plot, $^{31}P$ MAS spectrum; lower traces, $^{31}P\{^{27}Al\}$ REAPDOR difference spectra for evolution times $\tau = 429$, 571, 714, 1000, and 1429 $\mu$s (the most intense spectra correspond to the longer $\tau$ values).

concentration of Al increases. Hence, these experiments reveal no phase separation in this glass system.

*Pb−Al Metaphosphate.* Table 8 shows a compilation of $^{31}P$ and $^{27}Al$ NMR data for this system obtained in the same set of glasses used in ref 19. Newly improved $^{27}Al$ 3Q-MAS experiments were carried out in the present study using faster spinning rates and better signal-to-noise ratio than in ref 19. The resulting values for the parameters $^{27}Al$ $\delta_{CS}$ and $P_q$ are shown in Table 8. The values of both parameters for the Al(VI) sites are plotted in Figure 9, showing linear dependences with the Al concentration. For concentrations with $x > 0.4$ the values of $P_q$ are nearly identical to those observed in the alkali−Al systems.

Figure 10c shows an example of the $^{27}Al\{^{31}P\}$ REDOR result obtained in this glass system, corresponding to the glass


dx.doi.org/10.1021/jp205700j |J. Phys. Chem. C 2011, 115, 21927–21941

**Table 7. MAS-NMR Parameters for Na−Al Metaphosphate Glasses [a]**

| Na−Al molar fraction ($x$) | $^{31}$P $\delta_{CG}$ (ppm) | $Q^2_0$ | $Q^2_m$ | $^{27}$Al $\delta_{iso}$ (ppm) | $^{27}$Al $P_q$ (MHz) |
|---|---|---|---|---|---|
| 0 | −19.7 ± 0.2 | 1 | 0 | | |
| 0.06 | −22.4 ± 0.2 | 0.70 ± 0.05 | 0.25 ± 0.05 | VI, −13.0 ± 0.3 | 2.6 ± 0.2 |
| 0.08 | −22.8 ± 0.2 | 0.58 ± 0.05 | 0.41 ± 0.05 | VI, −13.7 ± 0.3 | 2.7 ± 0.2 |
| 0.10 | −23.7 ± 0.2 | 0.60 ± 0.05 | 0.38 ± 0.05 | VI, −13.3 ± 0.3 | 2.6 ± 0.2 |
| 0.12 | −25.0 ± 0.2 | 0.48 ± 0.05 | 0.52 ± 0.05 | VI, −12.5 ± 0.3 | 2.0 ± 0.2 |
| 0.15 | −25.4 ± 0.2 | 0.30 ± 0.05 | 0.70 ± 0.05 | VI, −14.0 ± 0.3 | 2.6 ± 0.2 |
| 0.18 | −26.6 ± 0.2 | 0.27 ± 0.05 | 0.73 ± 0.05 | | |
| 0.23 | −27.8 ± 0.2 | 0.20 ± 0.05 | 0.80 ± 0.05 | VI, −14.8 ± 0.3 | 2.6 ± 0.2 |
| 0.29 | −31.1 ± 0.2 | 0.18 ± 0.07 | 0.82 ± 0.07 | VI, −14.7 ± 0.3 | 2.5 ± 0.2 |
| | | | | V, 11.0 ± 0.5 | 2.4 ± 0.4 |
| 0.39 | −32.9 ± 0.2 | 0.07 ± 0.07 | 0.93 ± 0.05 | VI, −16.1 ± 0.3 | 3.2 ± 0.2 |
| | | | | V, 10.8 ± 0.5 | 3.3 ± 0.4 |
| 0.51 | −34.6 ± 0.2 | 0 | 1 | VI, −16.6 ± 0.3 | 3.4 ± 0.2 |
| | | | | V, 10.5 ± 0.3 | 2.7 ± 0.2 |
| | | | | IV, 41.0 ± 0.5 | 2.5 ± 0.5 |
| 0.61 | −36.8 ± 0.2 | 0 | 1 | VI, −17.6 ± 0.3 | 3.7 ± 0.2 |
| | | | | V, 10.7 ± 0.3 | 3.0 ± 0.2 |
| | | | | IV, 42.2 ± 0.5 | 3.2 ± 0.5 |
| 0.79 | −36.3 ± 0.2 | 0 | 1 | VI, −18.1 ± 0.3 | 4.1 ± 0.2 |
| | | | | V, 10.7 ± 0.3 | 3.6 ± 0.2 |
| | | | | IV, 41.7 ± 0.3 | 2.9 ± 0.4 |
| 0.90 | −38.1 ± 0.2 | 0 | 1 | VI, −18.3 ± 0.3 | 4.1 ± 0.2 |
| | | | | V, 9.5 ± 0.3 | 4.0 ± 0.2 |
| | | | | IV, 41.6 ± 0.3 | 3.2 ± 0.2 |

[a] $\delta_{CG}$: center of gravity of the $^{31}$P MAS-NMR line. $Q^2_0$ and $Q^2_m$: fractional populations of phosphate species determined from the $^{31}$P MAS-NMR spectra. $^{27}$Al $\delta_{iso}$ and $P_q$: isotropic chemical shift and second-order quadrupolar coupling product, respectively, determined from $^{27}$Al 3Q-MAS experiments for each kind of observed Al site (coordination VI, V, or IV).

with $x$ = 0.48. The parabolic analysis according to eq 3 yielded values for $M_2(^{27}\text{Al}\{^{31}\text{P}\})$, shown in Table 6, which are essentially identical within the experimental uncertainty. Therefore, as in the alkali metaphosphates, no variation can be detected in the P environment around Al.

Figure 12g,h,I shows the evolution of the $^{31}$P$\{^{27}$Al$\}$ REAPDOR signals for glasses with compositions $x$ = 0.08, 0.48, and 0.80. Figure 13e,f shows REAPDOR difference spectra for Pb−Al glasses with $x$ = 0.08 and 0.48. As a function of the dephasing time, the spectra for the $x$ = 0.08 glass have their maxima shifted to frequencies lower than the maximum in $^{31}$P MAS spectrum, reflecting that the phosphate units $Q^2_m$ ($m$ = 1, 2) are more strongly coupled to $^{27}$Al than the $Q^2_0$ groups. However, the latter units have nonzero dipolar coupling, as indicated by the extension of the $^{31}$P$\{^{27}$Al$\}$ REAPDOR difference spectra to the frequency region characteristic of these groups. This effect seems even more pronounced than in alkali−Al glasses. For this reason, as in the $x$ = 0.09 K−Al glass, the simple scaling of the two-spin simulation according to the $Q^2_m$ population cannot reproduce the evolution of the full REAPDOR signal. For the glass with $x$ = 0.48 (Figure 12h), the experimental REAPDOR data show an excellent agreement with the two-spin simulation without any scaling factor. As the estimated fraction of $Q^2_m$ in this glass is 0.94, the agreement indicates that phosphate units significantly coupled to $^{27}$Al are mostly of the $Q^2_1$ type. For the glass with $x$ = 0.80 (Figure 12i), the experimental data lie in between the three-spin and two-spin simulations, indicating that $Q^2_2$ and $Q^2_1$ species are contributing to the observed signal. Assuming a linear combination of these two REAPDOR simulations, the estimated populations for $Q^2_2$ and $Q^2_1$ result as 0.53 and 0.47, respectively.

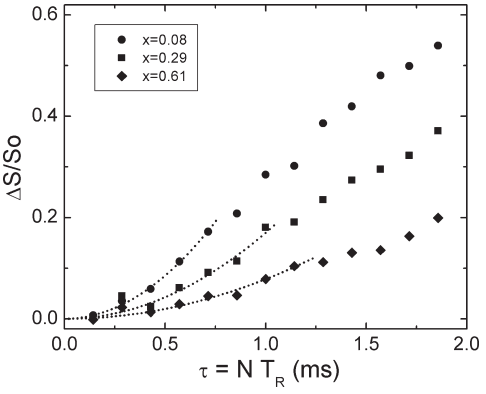


**Figure 14.** $^{31}$P$\{^{23}$Na$\}$ REDOR data for glasses in the Na−Al system with $x$ = 0.08 (circles), 0.29 (squares), and 0.61 (diamonds). Dotted lines: parabolic fittings according to expression 2.

## VI. DISCUSSION

**Phosphate Speciation.** In order to advance the description of the structure of the glass network of these systems, a quantitative analysis of the phosphate speciation as a function of the Al

**Table 8. MAS-NMR Parameters for Pb−Al Metaphosphate Glasses[a]**

| Pb−Al molar fraction ($x$) | $^{31}$P $\delta_{CG}$ (ppm) | $Q^2_0$ | $Q^2_m$ | $^{27}$Al $\delta_{iso}$ (ppm) | $^{27}$Al $P_q$ (MHz) |
|---|---|---|---|---|---|
| 0 | −25.7 ± 0.2 | 1 | 0 | | |
| 0.03 | −26.0 ± 0.2 | 0.86 ± 0.05 | 0.14 ± 0.05 | | |
| 0.08 | −27.1 ± 0.2 | 0.75 ± 0.05 | 0.25 ± 0.05 | VI, −15.9 ± 0.5 | 2.8 ± 0.3 |
| 0.15 | −29.0 ± 0.2 | 0.45 ± 0.05 | 0.55 ± 0.05 | VI, −16.6 ± 0.5 | 2.8 ± 0.3 |
| 0.25 | −30.9 ± 0.2 | 0.25 ± 0.05 | 0.75 ± 0.05 | VI, −16.4 ± 0.5 | 3.0 ± 0.2 |
| | | | | V, 10.0 ± 0.5 | 2.8 ± 0.4 |
| | | | | IV, 22.9 ± 0.5 | 3.6 ± 0.5 |
| 0.38 | −33.1 ± 0.2 | 0.12 ± 0.05 | 0.87 ± 0.05 | VI, −17.1 ± 0.5 | 3.3 ± 0.2 |
| | | | | V, 10.5 ± 0.5 | 2.9 ± 0.4 |
| | | | | IV, 42.9 ± 0.5 | 3.5 ± 0.5 |
| 0.48 | −34.5 ± 0.2 | 0.06 ± 0.05 | 0.94 ± 0.05 | VI, −17.4 ± 0.5 | 3.5 ± 0.2 |
| | | | | V, 9.5 ± 0.5 | 2.7 ± 0.4 |
| | | | | IV, 41.3 ± 0.5 | 3.1 ± 0.4 |
| 0.62 | −34.5 ± 0.2 | 0 | 1 | VI, −17.3 ± 0.5 | 3.6 ± 0.2 |
| | | | | V, 10.9 ± 0.5 | 3.2 ± 0.2 |
| | | | | IV, 42.8 ± 0.5 | 3.4 ± 0.2 |
| 0.73 | −36.4 ± 0.2 | 0 | 1 | VI, −18.5 ± 0.5 | 3.8 ± 0.2 |
| | | | | V, 10.2 ± 0.5 | 3.4 ± 0.2 |
| | | | | IV, 41.7 ± 0.5 | 3.2 ± 0.2 |
| 0.80 | −37.1 ± 0.2 | 0 | 1 | | |
| 0.85 | −37.5 ± 0.2 | 0 | 1 | VI, −18.4 ± 0.5 | 3.9 ± 0.2 |
| | | | | V, 10.1 ± 0.5 | 3.6 ± 0.2 |
| | | | | IV, 41.3 ± 0.5 | 3.3 ± 0.2 |
| 0.95 | −36.7 ± 0.2 | 0 | 1 | VI, −18.3 ± 0.5 | 4.1 ± 0.2 |
| | | | | V, 10.1 ± 0.5 | 3.6 ± 0.2 |
| | | | | IV, 41.3 ± 0.5 | 3.3 ± 0.2 |

[a] $\delta_{CG}$: center of gravity of the $^{31}$P MAS-NMR line. $Q^2_0$ and $Q^2_m$: fractional populations of phosphate species determined from the $^{31}$P MAS-NMR spectra. $^{27}$Al $\delta_{iso}$ and $P_q$: isotropic chemical shift and second-order quadrupolar coupling, respectively, determined from $^{27}$Al 3Q-MAS experiments for each kind of observed Al site (coordination VI, V or IV).

**Table 9. Populations of Phosphate Species ($Q^2_m$) Calculated According to the Segregation and Binary Distribution Scenarios, and the Probability ($p$) of Having a M−NBO (M = Na, K, Pb) Bond in the Random Bonding Scenario**

| glass | segregation | random bonding | binary distribution ($x < x_c$) |
|---|---|---|---|
| alkali−Al | $Q_0^2 = 1 - Q_2^2$ | $p = 2(1 - x)/[2(1 - x) + CN_{Al}x]$ | $Q_0^2 = 1 - Q_1^2$ |
| | $Q_2^2 = 3x/(1 - x + 3x)$ | | $Q_1^2 = (CN_{Al}x)/(1 + 2x)$ |
| Pb−Al | $Q_0^2 = 1 - Q_2^2$ | $p = 4(1 - x)/[4(1 - x) + CN_{Al}x]$ | $Q_0^2 = 1 - Q_1^2$ |
| | $Q_2^2 = 3x/[2(1 - x + 3x)]$ | | $Q_1^2 = CN_{Al}x/[2(1 - x) + 3x]$ |

content should be carried out. Three structural scenarios were considered here:

(I) segregation of individual metaphosphate-like environments, containing $Q^2_0$ and $Q^2_2$ phosphates;

(II) random bonding of all NBO with M or Al, with probability $p$ of having an M−NBO bond [The resulting population of phosphate species are determined by a binomial distribution: $Q^2_0 = p^2$, $Q^2_1 = 2p(1 - p)$ and $Q^2_2 = (1 - p)^2$, with $p$ given by the expressions in Table 9.];

(III) binary distribution, with only $Q^2_0$ and $Q^2_1$ species for glasses with low to middle Al concentrations and $Q^2_1$ and $Q^2_2$ for glasses with high Al concentration.

All scenarios have the implicit condition that no Al−O−Al linkages are formed in the glass.[17,19] The $^{27}$Al{$^{31}$P} REDOR results seem consistent with this assumption, because the measured $M_2(^{27}\text{Al}\{^{31}\text{P}\})$ values in the glasses are comparable with those measured for Al(VI) in the monoclinic $Al(PO_3)_3$ crystal (Table 5), where such bonds are not present.[32] Table 9 summarizes the expressions for phosphate populations and probabilities corresponding to each scenario for the alkali−Al and Pb−Al systems. The calculation of phosphate populations in the random and binary scenarios requires the knowledge of the average CN of Al, which is obtained directly from the interpolation of the data in Figure 8. In the case of the binary distribution, only the initial Al concentration range associated with the speciation $\{Q^2_0; Q^2_1\}$ was considered here, because only in this range can the results be directly compared with the experimental populations resolved by $^{31}$P NMR. The upper concentration limit $x_C$ for this regime corresponds to the condition of all $Q^2_0$ tetrahedra converted to $Q^2_1$, resulting for the alkali−Al systems as $x_C = 0.25$ and for the Pb−Al system as $x_C = 0.40$, if all the Al are six-coordinated. Owing to the slightly lower average coordination number of Al, the actual


dx.doi.org/10.1021/jp205700j |J. Phys. Chem. C 2011, 115, 21927–21941

$x_C$ values turn out to be slightly higher, amounting to 0.27 and 0.43, respectively, in the alkali−Al and the Pb−Al systems. The calculated fractions $Q^2_0$ and the sum $Q^2_1 + Q^2_2$, which is directly comparable with the NMR results, are plotted in Figure 7 for the three scenarios. As can be seen from these plots, the segregation scenario gives the poorest approximation to the observed populations in the three glass systems. This disagreement is not unexpected, considering that the linear behavior of the $^{31}$P and $^{27}$Al chemical shifts as a function of the Al concentration in the three systems strongly argue against phase separation. Therefore, it can be concluded that there is no segregation of $Al(PO_3)_3$-like regions in these glasses. On the other hand, the random bonding scenario agrees substantially better with the experimental data in the Na−Al system (Figure 7b). However, in the K−Al and Pb−Al systems, the binary scenario yields a better approximation to the experimental populations. This model also gives a closer approximation than the random bonding model in the Na−Al system, up to $x \sim 0.2$. Above that concentration, the systematic deviation of the model with respect to the populations determined experimentally indicates that some small fraction of $Q^2_2$ may be present in these Na−Al glasses as $x$ approaches $x_C$.

The random and binary models can also be tested considering the $^{31}P\{^{27}Al\}$ REAPDOR results. Figure 12 shows the REAPDOR curves (dashed lines) calculated as linear combinations of two- and three-spin simulations weighted with the $Q^2_1$ and $Q^2_2$ populations resulting from the random model. These curves were calculated only for the glasses with $x > 0.20$, which is where the populations obtained from both models differ appreciably. Also, at these compositions the effect of the $^{31}P-^{27}Al$ coupling of $Q^2_0$ groups has negligible influence on the results. For the Na−Al and Pb−Al glasses of intermediate $x$ (Figure 12e,h), the calculations based on the random model lie farther apart from the experimental results when compared with the two-spin simulations. The differences are even bigger in the glasses with the highest $x$ (Figure 12f,i), which indicates the inadequacy of the random model in this range of compositions. In the K−Al glasses (Figure 12b,c), the curves calculated from the random model populations are equally close to the experimental results as the two-spin scaled curve (Figure 12b) or the best linear combination of two- and three spins simulations (Figure 12c).

The overall evaluation of the performance of the models leads us to conclude that the binary model describes the experimental results better than the random model. However, the analysis at high Al concentrations is limited by the lack of direct resolution of the $Q^2_1$ and $Q^2_2$ populations to compare with the binary model calculation or with the weighting factors obtained in the simulation of the REAPDOR curves.

**Local Atomic Environments and Cation Dispersion.** For the Na−Al glasses, the values of $M_2(^{23}Na\{^{31}P\})$ determined from $^{23}Na\{^{31}P\}$REDOR experiments (Table 6) do not provide any evidence of major structural rearrangements in the local P environment around Na. This observation points to an essentially invariant local environment around Na, independent of the Al concentration.

Regarding the local structure around Al, the similar magnitude of $M_2(^{27}Al\{^{31}P\})$ in the set of analyzed glasses may indicate a certain structural similarity in the environments of P around Al. In crystalline $Al(PO_3)_3$, there are six close phosphate tetrahedra around the Al(VI) sites.[32] The $M_2(^{27}Al\{^{31}P\})$ value obtained for this compound is $(5.4 \pm 0.2) \times 10^6$ rad$^2$ s$^{-2}$, which is close to the values determined for Al(IV), Al(V), and Al(VI) sites in the $Al(PO_3)_3$ glass. On the basis of this similarity, there is no experimental evidence for the formation of Al−O−Al bonds in the glass. The same conclusions may be extended to the rest of the analyzed glasses, according to the similarity of the $M_2(^{27}Al\{^{31}P\})$ values in Table 6. This result supports two of the basic assumptions used to describe the structure of ternary phosphate glasses:[17−19] the absence of Al−O−Al bridges and the linkage between $PO_4$ and $AlO_n$ polyhedra through corners instead of edges or faces. These properties of the medium-range order are compatible with previous models proposed for binary ultraphosphate glasses.[16]

The linear evolution observed for the $^{27}$Al chemical shift in the three glass systems indicates atomic-scale mixing of this species with the second cation. This observation is consistent with the absence of segregation in $Al(PO_3)_3$-like regions determined from the analysis of the $Q^2_m$ populations. According to Figure 9a, the values of $^{27}$Al $\delta_{CS}$ follow two well-defined trends with composition. First, in all systems there is a decrease in the $^{27}$Al $\delta_{CS}$ values of Al(VI) with the increase in the Al concentration. This trend is consistent with the process of charge redistribution proposed by Metwalli and Brow to explain the decrease in the Al CN observed in aluminum metaphosphates,[35] which is a behavior also observed in these three glass systems. According to their description, as the M−NBO bonds (M = K, Na, or Pb) are substituted by less ionic Al−NBO bonds, more charge transfer is required from other Al neighbors to P. This process should shift the $^{27}$Al resonance to lower frequencies, as experimentally observed. Also, the average coordination of Al is expected to decrease, as the charge transfer from Al(IV) is greater than that from Al(VI).[35] The second trend observed in Figure 9a for $^{27}$Al $\delta_{CS}$ values is their dependence on the second cation species, with chemical shifts decreasing in the sequence $\delta_{CS}(K-Al) > \delta_{CS}(Na-Al) > \delta_{CS}(Pb-Al)$, when considering glasses with the same Al concentration. This behavior is correlated with the increase in the ionic potential, defined as the valence divided by ionic radii given by Shannon and Prewitt,[36] 0.72 Å$^{-1}$ for $K^+$, 0.98 Å$^{-1}$ for $Na^+$, and 2.13 Å$^{-1}$ for $Pb^{2+}$, and can be explained by an analogous charge distribution process as described above. It is interesting to note that the differences in charge transfer in K−Al and Na−Al glasses are not as strong as to cause appreciable differences in the Al CN (Figure 8), but they are clearly revealed by differences in the $^{27}$Al chemical shifts (Figure 9a). On the other hand, the values of Al CN for the Pb−Al system are systematically lower than those for the alkali−Al glasses. This behavior is also a consequence of the charge transfer mechanism described previously, as Pb−O bonds are considerably less ionic than Na−O and K−O bonds.[35]

The values of the average $^{27}$Al quadrupolar coupling parameter $P_q$ increase with increasing Al concentration in the three glass systems, as seen in Figure 9b. For concentrations with $x > 0.40$, all the values converge to the same linear evolution observed in Pb−Al glasses, within the uncertainty of the determination. Only for those glasses with the lower concentrations of Al, the $P_q$ values in alkali−Al glasses seem slightly smaller than in Pb−Al. These results suggest that the nature of the second chemical species (Na, K, or Pb) has a weak effect in determining the local geometry of the Al(VI) sites.

## V. CONCLUSION

The findings presented here indicate the existence of nonrandom bonding between the NBO and the two cation species in ternary aluminophosphate systems, in accordance with the bond

preferences observed in binary phosphates. The $^{27}Al\{^{31}P\}$ REDOR experiments in the three glass systems indicate that the environments of Al have many close P atoms, with second moment values of $^{27}Al\{^{31}P\}$ dipolar coupling equivalent to that measured in crystalline $Al(PO_3)_3$. This similarity points to a local structure in the glass without Al−O−Al bonds and with Al- and P-coordination polyhedra probably sharing only corners. The $^{23}Na\{^{31}P\}$ REDOR experiments reveal that the local phosphate environment around the Na sites is invariant, irrespective of the Al concentration. The local geometry of the Al(VI) sites is essentially insensitive to the nature of the second cation ($Na^+$, $K^+$, or $Pb^{2+}$) but strongly dependent on the concentration of Al in the glass. The average coordination number for Al decreases as more covalent M−O bonds, with M = Pb or Al, are present in the glass. A common behavior in the phosphate speciation is inferred in the Na−Al, K−Al, and Pb−Al glass systems. The analysis of the phosphate populations and the $^{31}P\{^{27}Al\}$ REAPDOR experiments in the three systems show that up to intermediate Al concentrations the association of P with Al occurs preferentially through one NBO per phosphate tetrahedron, (i.e., forming $Q^2_1$ units). For glasses with higher Al content, all P are associated with a close Al either through one or two NBO, yielding a $\{Q^2_1, Q^2_2\}$ speciation. In particular, the existence of cation segregation in these glasses can be discounted. The quantitative analysis of the phosphate populations shows that the distribution is close to binary $\{Q^2_0,Q^2_1\}$ for K−Al and Pb−Al glasses. In the Na−Al system, the observed speciation deviates from the binary distribution at intermediate concentrations of Al, indicating the presence of a small fraction of $Q^2_2$ coexisting with $Q^2_0$ and $Q^2_1$.

## ■ ASSOCIATED CONTENT

**Supporting Information.** Additional information as noted in the text. This material is available free of charge via the Internet at http://pubs.acs.org.

## ■ AUTHOR INFORMATION

**Corresponding Author**
*E-mail: schnei@ifsc.usp.br.

## ■ ACKNOWLEDGMENT

Support from FAPESP (grant 06/61218-0), DFG-Sonderforschungsbereich SFB 458, CNPq, and CAPES is gratefully acknowledged. M.T.R. is grateful for a personal fellowship by the Fonds der Chemischen Industrie and the Studienstiftung des Deutschen Volkes.

## ■ REFERENCES

(1) Peng, Y. B.; Day, D. E. *Glass Technol.* **1991**, *32* (6), 166–173.
(2) He, Y.; Day, D. E. *Glass Technol.* **1992**, *33* (6), 214–219.
(3) Donald, I. W. *J. Mater. Sci.* **1993**, *11*, 2841–2886.
(4) Hunt, J. T.; Speck, D. R. *Opt. Eng.* **1989**, *28*, 461–468.
(5) Jiang, S.; Myers, M.; Peyghambarian, N. *J. Non-Cryst. Solids* **1998**, *239*, 143–148.
(6) Dai, S.; Sugiyama, A.; Hu, L.; Liu, Z.; Huang, G.; Jiang, Z. *J. Non-Cryst. Solids* **2002**, *311*, 138–144.
(7) Donald, I. W.; Metcalfe, B. L.; Taylor, R. N. J. *J. Mater. Sci.* **1997**, *22*, 5851–5887.
(8) Donald, I. W.; Metcalfe, B. L. *J. Non-Cryst. Solids* **2004**, *348*, 118–122.
(9) Abou Neel, E. A.; Pickup, D. M.; Valappil, S. P.; Newport, R. J.; Knowles, J. C. *J. Mater. Chem.* **2009**, *19*, 690–701.
(10) Brow, R. K. *J. Am. Ceram. Soc.* **1993**, *76* (4), 913–918.
(11) Brow, R.; Kirkpatrick, R. J.; Turner, G. L. *J. Am. Ceram. Soc.* **1993**, *76* (4), 919–928.
(12) Lockyer, M. W. G.; Holland, D.; Howes, A. P.; Dupree, R. *Solid State Nucl. Magn. Reson.* **1995**, *5*, 23–34.
(13) Eckert, H. *Prog. NMR Spectrosc.* **1992**, *24* (3), 159–293.
(14) Van Wazer, J. R. *Phosphorus and Its Compounds*; Interscience: New York, 1958; Vol. 1.
(15) Brow, R. *J. Non-Cryst. Solids* **2000**, *263 & 264*, 1–28.
(16) Hoppe, U. *J. Non-Cryst. Solids* **1996**, *195*, 138–147.
(17) Schneider, J.; Oliveira, S. L.; Nunes, L. A. O.; Panepucci, H. *J. Am. Ceram. Soc.* **2003**, *86*, 317–324.
(18) Schneider, J.; Oliveira, S. L.; Nunes, L. A. O.; Bonk, F. *Inorg. Chem.* **2005**, *44*, 423–430.
(19) Tsuchida, J. E.; Schneider, J.; Pizani, P. S.; Oliveira, S. L. *Inorg. Chem.* **2008**, *47*, 690–698.
(20) Dollase, W.; Merwin, L.; Sebald, A. *J. Solid State Chem.* **1989**, *83*, 140–49.
(21) Wegner, S.; van Wüllen, L.; Tricot, G. *J. Non-Cryst. Solids* **2008**, *354*, 1703–1714.
(22) Zhang, L.; Eckert, H. *Solid State Nucl. Magn. Reson.* **2004**, *26*, 132–146.
(23) Zhang, L.; Eckert, H. *J. Phys. Chem. B* **2006**, *110*, 8946–8958.
(24) van Wüllen, L.; Tricot, G.; Wegner, S. *Solid State Nucl. Magn. Reson.* **2007**, *32*, 44–52.
(25) Amoureux, J. P.; Fernandez, C.; Steuernagel, S. *J. Magn. Reson. A* **1996**, *123*, 116–118.
(26) Massiot, D.; Touzo, B.; Trumeau, D.; Coutures, J. P.; Virlet, J.; Florian, P.; Grandinetti, P. J. *Solid State Nucl. Magn. Reson.* **1996**, *6*, 73–83.
(27) Strojek, W.; Kalwei, M.; Eckert, H. *J. Phys. Chem. B* **2004**, *108*, 7061–7073.
(28) Bak, M.; Rasmussen, J. T.; Nielsen, N. C. *J. Magn. Reson.* **2000**, *147*, 296–330.
(29) Gullion, T.; Schaefer, J. S. *J. Magn. Reson.* **1989**, *81*, 196–200.
(30) Chan, J. C. C.; Eckert, H. *J. Magn. Reson.* **2000**, *147*, 170–178.
(31) Gullion, T. *J. Magn. Reson.* **1995**, *A117*, 326–329.
(32) van der Meer, H. *Acta Crystallogr.* **1976**, *B32*, 2423–2426.
(33) Rinke, M. T.; Zhang, L.; Eckert, H. *Chem. Phys. Chem.* **2007**, *8*, 1988–1998.
(34) Brow, R. K.; Kirkpatrick, R. J.; Turner, G. L. *J. Am. Ceram. Soc.* **1990**, *73*, 2293–2300.
(35) Metwalli, E.; Brow, R. K. *J. Non-Cryst. Solids* **2001**, *289*, 113–122.
(36) Shannon, R. D.; Prewitt, C. T. *Acta Crystallogr.* **1969**, *B25*, 925–946.